Current-Voltage Characterisation of Monolayer-Supported Au-Nanoclusters by Scanning Tunnelling Microscopy under Ambient Conditions

Volker Jacobsen,[a,b] Tao Zhu,[a,c] Wolfgang Knoll,[a] and Maximilian Kreiter*[a]

Keywords: Scanning probe microscopy / Surface plasmon resonance / Colloids / Monolayers / Nanostructures / Self-assembly

The current-voltage characteristics of a double-tunnel junction based on a gold crystallite with a diameter of ca. 2 nm, separated from a gold surface by ca. 1 nm was investigated by scanning tunnelling microscopy. The sample architecture was built by attaching gold nanoparticles covered with 2-mercaptosuccinic acid to an atomically flat gold surface which was covered by a self-assembled monolayer (SAM) of 6-amino-1-hexanethiol. Surface plasmon and infrared spectroscopy as well as STM imaging were employed to identify suitable preparation conditions and prove the existence of the desired architecture. No reproducible steps in the current-voltage characteristics are observed on this system under ambient conditions. Nonetheless, a sound signature for tunnelling through the double-tunnel junction is established by a quantitative fit of the averaged experimental data to a theoretical model of a single-tunnel junction. Firstly, the current on the particle is strongly reduced at low absolute external voltage and secondly the current voltage characteristics are asymmetric. Since both deviations from theory are absent in reference experiments on the bare monolayer, they may serve as a robust signature for double-tunnel junctions and open the door to the investigation of single-electron tunnelling under ambient conditions.

Introduction

The quantization of the electrical current into individual electron charges leads to unique features in the current-voltage characteristics of double-tunnel junctions in which the current flows across an isolated island with a sufficiently small capacitance. In many cases this geometry is realised by the tip of a scanning tunnelling microscope (STM), approaching a metallic nanoparticle, which is isolated from a metallic substrate by a thin isolating layer with a thickness in the nanometer range.[1] This geometry is shown schematically in Figure 1. A complete suppression of current at small applied voltages and a jump to a finite current at a well-defined bias voltage are observed in low temperature experiments, the "Coulomb blockade". If the voltage is further increased, then more current jumps, at a defined voltage spacing, are observed. This feature is termed "Coulomb staircase". Both effects are understood in terms of the charging of the island by single electrons, which leads to a change in its electrostatic potential, resulting in discrete electronic states spaced out in energy. The position of the jumps depends on the geometry of the double-tunnel junction (capacitance of the particle, resistance of the two-tunnel junctions) as well as the offset potential of the island.[2] This potential, although in general due to the charge distribution in the vicinity of the island, is commonly expressed in terms of an equivalent "background charge" which is not quantized and residing on the island itself. It leads to a corresponding shift in electronic potentials and, in turn, to a shift of the applied voltages for which current jumps are

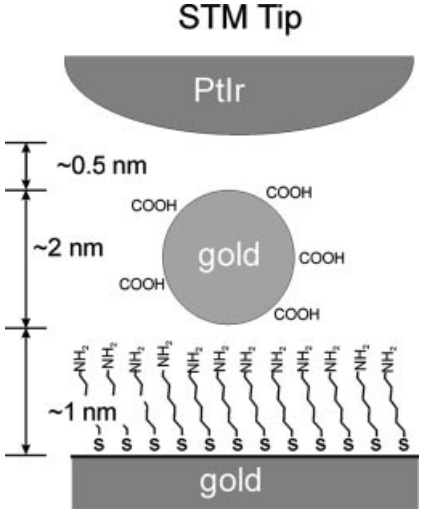

Figure 1. Sketch of a double-tunnel junction with an STM tip, an isolated metal nanoparticle and a monolayer-coated conducting substrate.

[a] Max Planck Institut für Polymerforschung,
Ackermannweg 10, 55128 Mainz, Germany
E-mail: kreiter@mpip-mainz.mpg.de
[b] Current address: Laboratory of Physical Chemistry, Swiss Federal Institute of Technology (ETH),
8093 Zurich, Switzerland
[c] Permanent address: College of Chemistry, Peking University,
Beijing 100871, China

observed. At a finite temperature, the sharp jumps are smeared out in energy on a scale corresponding to the thermal energy. As a consequence, the small steps in energy on systems with a large capacitance (small charging energy) are only observed at low temperature. Room temperature corresponds to a thermal energy of 25 meV. For this reason, only Coulomb blockades on small particles with correspondingly small capacitance can be observed in this temperature regime. An elegant route to small gold particles in a well-defined distance from a conducting substrate is based on the use of self-assembled monolayers as spacer molecules whose thickness can be adjusted to the Angstrom scale and on top of which gold nanoparticles with the appropriate size are deposited.

Several combinations of substrates, particles and organic functionalities of self-assembled monolayers have been used for such studies.

One strategy is based on the deposition of metallic particles coated by an insulating material on bare conducting substrates such as Pt_{309}phenanthroline$_{36}O_{30}$[3] and hexanethiol-capped clusters[4] on clean Au(111) as well as polyvinylpyrrolidone capped Au particles on graphite.[5]

Similarly, bare particles can be deposited on a monolayer-protected surface as was shown for clusters prepared under ultrahigh vacuum (UHV),[6,7] which were deposited on Au(111) protected by a monolayer of *p*-xylene-α-α′-dithiol ($C_8H_{12}S_2$). It must be noted, though, that this approach is restricted to vacuum techniques, since in ambient environments metal clusters need some stabilizing agents, thus preventing the use of bare clusters.

Probably, the best-defined systems are prepared by using a specific organic coating both on the particle and on the substrate, thus avoiding any influence of loosely bound contaminants. Examples for this strategy are heptanethiol-capped clusters on Au(111) coated with a decanethiol self-assembled monolayer,[8] and dodecanethiol-coated particles on Au(111) protected by a monolayer of *p*-xylene-α-α′-dithiol ($C_8H_{12}S_2$).[9] Other experiments on clusters coated with octanethiol/galvinol/mecaptohexylamine on Au coated by hexanethiol[10,11] have been reported.

Most of these experiments were performed under UHV at low temperatures[3,8,12] thus avoiding a smearing out of the steps in the $I(V)$ curve while at the same time avoiding fluctuations of the background charge by immobilizing possible contaminations. Also, at room temperature, Coulomb staircases have been measured under UHV and the results are in agreement with a modified classical theory that takes into account the thermal contribution.[7,12,13]

The high sensitivity of $I(V)$ on the background charge makes the detection of clear $I(V)$ curves under ambient conditions very difficult since all kinds of contaminations will enter and leave the vicinity of the tunnel barrier, leading to a background charge fluctuating quicker in time than the time needed for an $I(V)$ curve. On the other hand, this high sensitivity makes the measurement of single-electron tunnelling events a promising candidate for true transduction of single-molecular switching events if they are accompanied by a change in the associated electrostatic potential.[14] The feasibility of single-electron charging experiments at ambient conditions has been shown by addressing single clusters with an STM tip[10,11,15] and in an electrochemical experiment which was supplemented by STM experiments under UHV.[4] Still, in these cases no quantitative comparison to the classical theory was shown, probably due to the high temporal fluctuations in the overall architecture. It was noted that charged coatings may lead to an increased fluctuation of the background charge,[5] which was corroborated by the remarkable quality of the data from purely aliphatic SAMs.[8] Furthermore, in a polar environment a dielectric response has to be considered that reacts on time scales that are similar or slower than some of the time scales relevant for the experiment. As a consequence, the dynamics of the reorientation of polar species must be considered, leading to additional deviations from the simple picture of a static system with instantaneous dielectric response.[16]

Nonetheless, there are two important reasons to choose charged coatings of the particles and the substrate. Firstly, in order to attach further molecular functionalities some reactivity of the particle coatings is required. Secondly, at ambient conditions the immobilization has to withstand displacement by other molecules and therefore requires some robustness.

In this paper, we are investigating carboxyl-functionalized Au-nanoclusters on an amino-functionalized SAM in air. The goal of this paper is to unravel signatures of tunnelling through a double-tunnel junction in this polar system using STM experiments at ambient conditions. Firstly, the supramolecular geometry consisting of a 6-amino-1-hexanethiol monolayer bound to a gold substrate, decorated by gold nanoparticles coated with mercaptosuccinic acid (MSA) is thoroughly characterized. Scanning tunnelling investigations are shown with an emphasis on the changes of the $I(V)$ characteristics with time. Based on the observation that no reproducible step position of a Coulomb staircase can be identified, an alternative, fully reproducible signature of the $I(V)$ characteristics through a double-tunnel junction is developed which may serve as a signature of single-electron tunnelling even in a strongly fluctuating environment such as ambient air.

Results and Discussion

FTIR and Surface Plasmon Investigations

The deposition of the spacer layer as monitored by surface plasmon spectroscopy is displayed in Figure 2. The evolution of the minimum angle as a function of time (Figure 2b) indicates a quick first adsorption process, which terminates roughly at a thickness corresponding to a self-assembled monolayer of the 6-amino-1-hexanethiol. This process is followed by a second, slower deposition. The reflectivity curves in Figure 2a show that this additional thickness does not decrease upon rinsing with Milli-Q water, indicating a relatively strong affinity. Upon rinsing with 0.1 M HCl, the adlayer thickness is reduced to its value after the first quick deposition. This can be explained by

some additional 6-amino-1-hexanethiol molecules on top of the first monolayer, which are attached by dimerisation of the head amino groups and are removed after protonation in an acid environment.

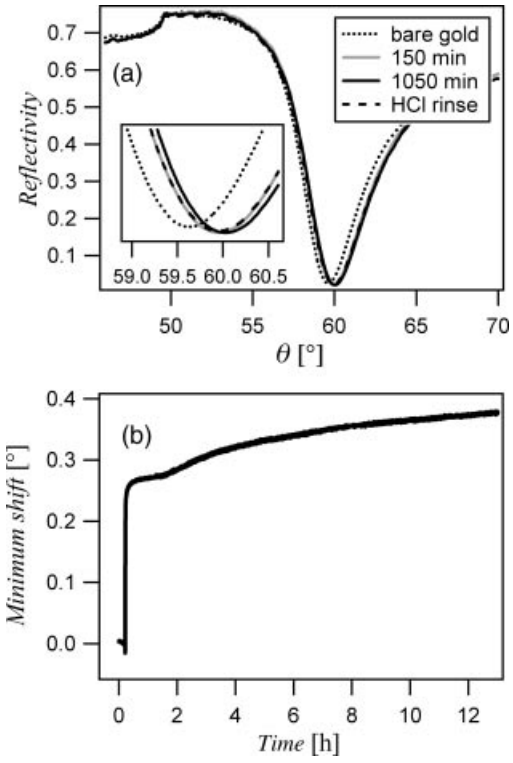

Figure 2. Surface plasmon investigation of the monolayer formation. (a) Reflectivity curves before deposition of 6-amino-1-hexanethiol, after 150 min and 1050 min deposition time and after rinsing with 0.1 M HCl, respectively. (b) Minimum angle shift as a function of time. In this range, the shift in the minimum angle is proportional to the surface coverage.

FTIR spectra of the gold substrates were taken after immersion in the thiol solution and after the rinsing steps. They are displayed in Figure 3.

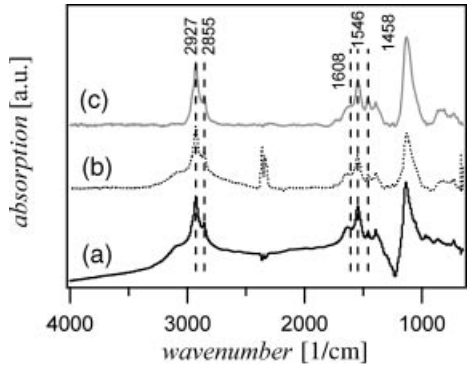

Figure 3. FTIR Spectra of the gold substrate (a) after immersion in the solution containing the 6-amino-1-hexanethiol (b) after rinsing with Milli-Q water (c) after rinsing with 0.1 M HCl.

The characteristic bands for a CH_2 chain are observed: an asymmetric stretching mode at 2927 cm^{-1} and a symmetric stretching mode at 2855 cm^{-1}, as well as a CH_2 scissoring band at 1458 cm^{-1}. The stretching modes are slightly shifted to higher wavenumbers compared to values obtained in solution (2924 cm^{-1} and 2853 cm^{-1}[17]) and in agreement with values found for a disordered monolayer with a density below the one found for the ideal crystalline packing of longer alkanethiols.[18] This finding is reasonable taking into account the influence of the amino head group and the relatively short alkyl chain whose energy in the chain-chain interactions is insufficient to form a 2D crystal. Peaks at 1546 cm^{-1} and at 1608 cm^{-1} are identified as the symmetric and asymmetric NH_3^+ deformation of the amine salt.

It is worth noting that some background signal is obtained before rinsing with HCl. This is attributed to the additional material which is also observed in surface plasmon spectroscopy and is interpreted in terms of additional 6-amino-1-hexanethiol molecules that bind to the self-assembled monolayer by dimerisation of the amino groups and which can be removed in an acid environment. A somewhat ill defined formation of SAMs from amino-terminated thiols is known from the literature. The formation of double layers has been reported,[19] as well as proper single SAMs[20,21] with the formation of carbamate at ambient conditions.[20] There is a possibility of a reverse incorporation of some molecules, i.e. the amino group pointing in the direction of the gold has been reported.[22] In the case discussed here, the clean IR spectrum as well as the thickness, corresponding to a self-assembled monolayer determined by surface-plasmon spectroscopy, point to the existence of a well-defined self-assembled monolayer after rinsing with HCl. From the IR spectra as well as from the observation that no molecular ordering could be resolved with the STM, a disordered monolayer can be deduced.

The deposition of MSA-capped gold particles was monitored in situ by surface plasmon spectroscopy as displayed in Figure 4. After 30 min the deposition speed slows down significantly but does not saturate completely even within 16 h, indicating a slow on-going particle aggregation after saturation of the main binding sites. Rinsing with HCl reduces the amount of Au particles by roughly 30% pointing to the removal of some weakly bound material. Remarkably, in addition to the horizontal shift of the plasmon curve, a slight broadening is observed, which may point towards an increased aggregation of loosely bound particles induced by the rinsing, which is expected to cause significant scattering and therefore an increase in optical absorption.

After deposition of the MSA-capped gold particles, bands at 1719 cm^{-1}, 1578 cm^{-1}, and 1392 cm^{-1} appear in the FTIR spectra (Figure 5), indicating the presence of carboxylic groups on the surface and therefore pointing towards successful deposition of the gold particles.

Imaging of the Particles with the STM

STM images of the substrates with immobilized gold nanoparticles are displayed in Figure 6. Atomically flat

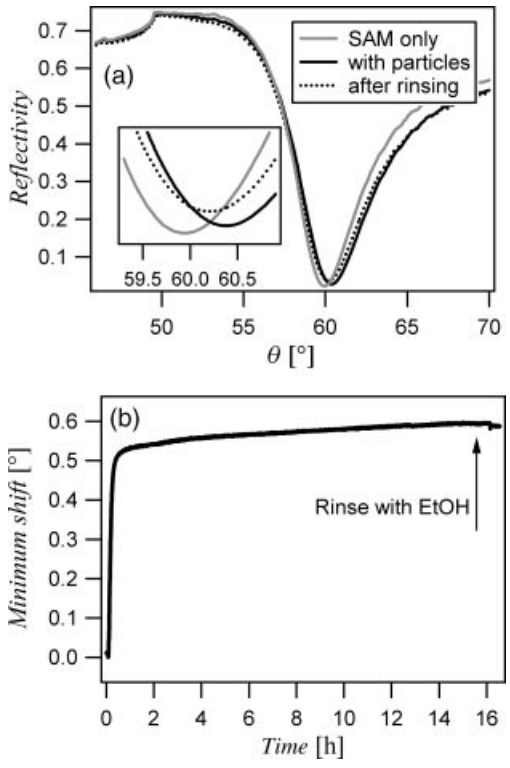

Figure 4. Surface plasmon investigations on particle deposition. (a) Surface plasmon reflectivity curves before and after particle deposition and after rinsing. (b) Kinetics of gold particle deposition.

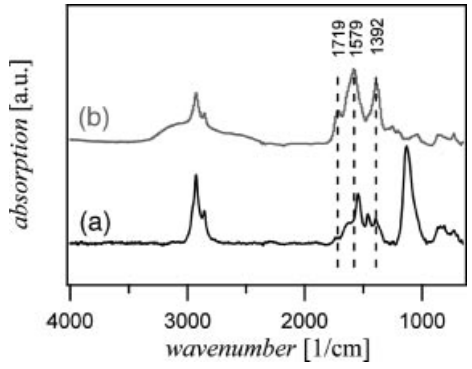

Figure 5. FTIR spectra before (a) and after (b) deposition of Au nanoparticles.

gold terraces with lateral dimensions in the order of 100 nm are clearly seen in Figure 6a. Some particles are only partly visible in the image because they are swept away by the STM tip, these features are indicated by arrows. Figure 6b is obtained at slightly increased bias voltage and a set point current decreased to less than half the value used for the image in (a). Under these conditions stable imaging of the particles is achieved due to the increased distance of the tip to the surface.[23] An image taken on a single particle at reduced image size is shown in Figure 6c with a line profile across the particle displayed in Figure 6d. Firstly it can be seen that the particle has an apparent height of roughly 1.5 nm, which gives an estimate for the real dimension of the particle. Different I(z) characteristics on the particle and on the substrate, may lead to an error of some Angstroms in this height estimate. The apparent lateral size of 6 nm is dominated by the convolution with the geometrical shape of the tip and can therefore only provide an upper limit for the particle size. The surface of the gold terrace appears to be modulated in the range of roughly 1 Å, pointing towards a noncrystalline morphology of the amino-terminated thiol monolayer in agreement with the FTIR investigations. Atomic force microscopy was applied as a complementary method to investigate the surface topography independent from its electric response and an apparent particle height and density was found which was consistent with the results from the STM investigations.

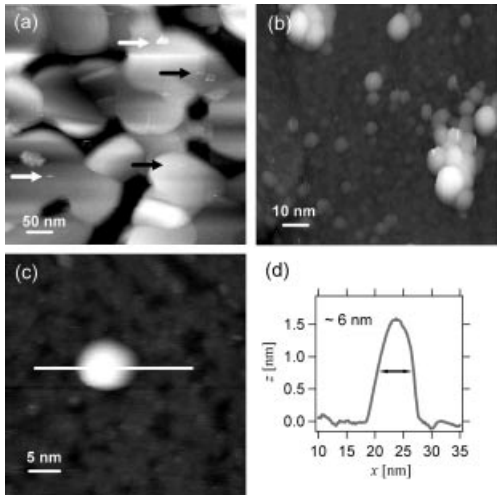

Figure 6. STM images. (a) The arrows indicate particles that are swept away during the imaging (401 mV, 93.4 pA). (b) Decreased tunnel current (500 mV, 38.5 pA). (c) Close-up of (b) (500 mV, 40.7 pA). (d) Line profile through (c).

Spectroscopy was performed by choosing an image frame such that one single particle covers roughly 50% of the image area as shown in Figure 7a, while reference measurements were taken on the same sample for an area without particles. Averaged $I(V)$ curves are displayed in Figure 7b, showing no significant difference between the two experiments, particularly, no pronounced steplike feature as is expected for a Coulomb blockade effect is observed. Single $I(V)$ curves taken on a particle are displayed in Figure 7c and are to be compared with the $I(V)$ curves taken on the pure SAM displayed in Figure 7d. These curves were chosen in a random fashion, i.e. no selection criteria were applied.

Both sets of curves show some differences in the shape of the individual curves, such as a significantly increased current in the uppermost curve in Figure 7d. The saturation at high negative currents is due to the maximum output of the electronics and does not reflect a real physical effect. Typical features of the individual curves taken on the particle are both steplike features as indicated by the vertical lines in the lowest curve and sudden "reverse" jumps which appear as an effective decrease in current at increasing voltage and are marked by arrows in two curves. The individual curves taken on the SAM do not show such behaviour.

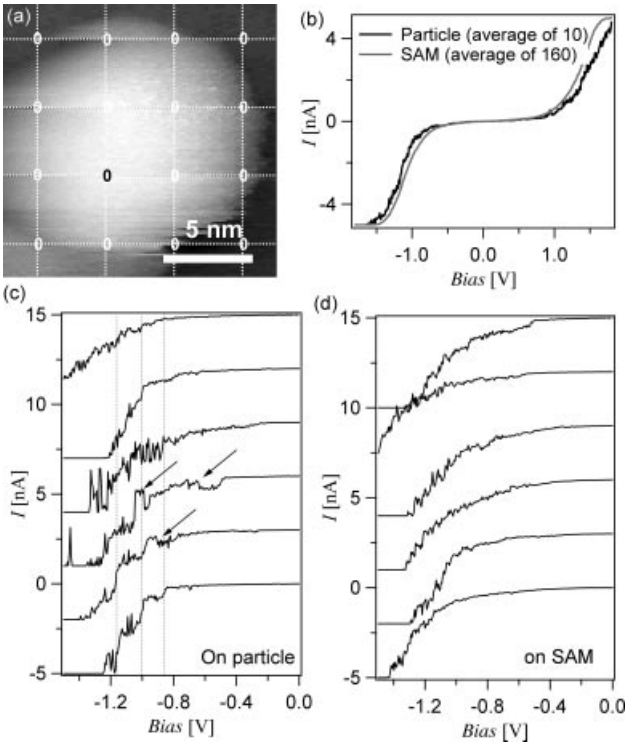

Figure 7. (a) Scanning tunnelling image of a Au nanoparticle (image size 15×15 nm^2). At the indicated 16 points, $I(V)$ spectra were taken during image acquisition (bias = 502 mV, I = 34 pA). (b) Average of 10 $I(V)$ curves obtained, indicated by the position marked in black in (a) compared to the average of all 160 $I(V)$ curves obtained with identical parameters (bias = 502 mV, I = 42.7 pA) on the same sample with no gold particles in the image range. (c) Sequence of individual curves obtained at the position marked by the black "0" in (a). The first six curves that were recorded are displayed, i.e. the data is chosen randomly. The features marked by the arrows and by the vertical dashed lines are explained in the text. (d) Sequence of individual curves randomly chosen from the spectra measured on a sample area without particles and averaged in (b). The curves in (c) and (d) are offset for clarity.

Similar current-voltage steps in single $I(V)$ curves were observed under ambient conditions[10,11,15] and have been assigned to a Coulomb staircase. In the system studied here, a reproducible measurement of the steplike features in the $I(V)$ curve was not possible, thus preventing a clear discrimination as to whether the steps are due to a Coulomb blockade or due to fluctuations of the background charge. The irreproducibility of the $I(V)$ curves as well as the "reverse jumps" may be interpreted as fluctuations of either the background charge or the entire double-tunnel-junction geometry with time, which occurs with high probability in polar systems.[5] On average a smooth $I(V)$ curve is obtained (see Figure 7b) when averaging over a set of experiments and all steplike features are averaged out.

The dI/dV curves acquired simultaneously with the data displayed in Figure 7c and d are shown in Figure 8a and b, respectively. On the SAM, no clear features are seen in the dI/dV representation in agreement with the observations on the $I(V)$ data. The individual curves taken on the particle show some features, which may be interpreted as maxima. They are again highly irreproducible from measurement to measurement. A comparison of the voltage for which apparent steps in the $I(V)$ data occur is made by marking the corresponding voltages in both Figure 7c and Figure 8a. No clear correlation is seen, giving additional evidence that extraction of Coulomb staircase-like behaviour from these experiments is either impossible or would require a very deep and careful statistical analysis.

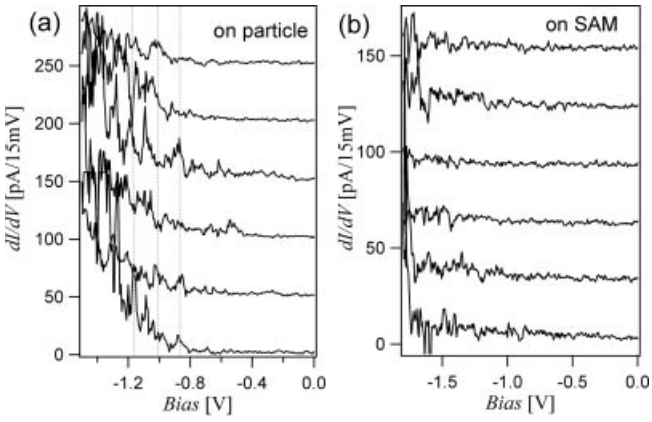

Figure 8. Single scans of the differential conductivity on the particle (a) and on the SAM (b). These data were obtained simultaneously with the curves in Figure 7c and d.

For this reason, an attempt is made with the following to extract information from the only data that can be obtained in a reproducible manner i.e. the averaged curves. Either $I(V)$ or dI/dV may be used for the analysis since they contain redundant information, though the observed effects are better visible with the dI/dV curves, which are therefore discussed below. Such averaged curves taken on a particle and on the SAM are shown in Figure 9a and b and Figure 9c and d, respectively.

A quantitative evaluation of these curves is done by comparing it to a fit based on an approach by Ukraintsev[24] for a single tunnel junction based on the one-dimensional WKB approximation which assumes comparable average density of states at the Fermi level for the tip and sample. This method, originally proposed as the "density of states deconvolution technique" is applied here to quantify the deviation from a normal response of a metal-metal contact. Following Ukraintsev, the measured dI/dV signal can be expressed as

$$\frac{\mathrm{d}I}{\mathrm{d}V}(z,V) = \frac{eA}{2}[T(z,eV/2) + T(z,-eV/2)] \quad (1)$$

with

$$T(z,\xi) = \exp[-2z\frac{8\pi^2 m_e}{\hbar^2}(\bar{\Phi} - \xi)] \quad (2)$$

Where e, m_e, $\hbar$ are the electron charge and mass and Planck's constant respectively, z the tunnelling distance, V the voltage, A a scaling parameter for the absolute value of the tunnel current and $\bar{\Phi}$ the average of the work functions of the tip and substrate material (Φ = 5.31 eV for Au.[25] An identical value is assumed for the Pt/Ir 90:10 alloy that the tip is composed of, based on the literature values of

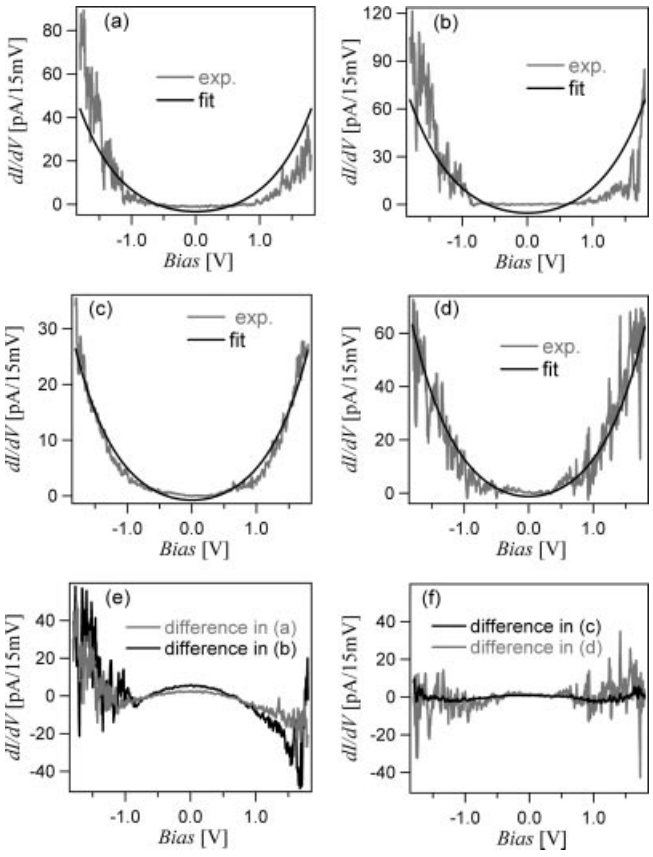

Figure 9. (a) and (b) dI/dV spectra obtained on two different gold nanoparticles The curves are averaged over 10 individual data sets and are representative of 20 particles that were studied. The fit of Equations 1 and 2 to the data using the approach of Ukraintsev is shown as a solid line. The fitting parameters are (d = 1.17 nm, A = 4.29×10^9 V s^{-1}) for (a) and (d = 1.11 nm, A = 1.63×10^9 V s^{-1}) for (b). (c) and (d) were obtained under identical experimental conditions as (a) and (b) on the bare SAM. (c) and (d) are averaged over 150 and 10 individual curves, respectively. The fitting parameters are (d = 1.2 nm, A = 3.92×10^9 V s^{-1}) for (c) and (d = 1.13 nm, A = 2.1×10^9 V s^{-1}) for (d). (e) Residual of the two fits of the gold particle in (a) and (b). (f) Residual of the two fits of the SAM in (c) and (d).

5.65 eV (Pt) and 5.27 eV (Ir)[25]). The remaining free parameters in this fit are the tunnel distance z and the overall scaling parameter A.

A good agreement of the fit with the experimental data was obtained on the pure SAM (Figure 9c and d), justifying the simplifications made by the model a posteriori. The difference spectra (Figure 9f) display only negligible deviations. This good agreement of the Ukraintsev-model, which assumes tunnelling through a vacuum, with our data is remarkable. It shows that a good fit is obtained, although instead of a vacuum, an amino-functionalized thiol is located in the tunnel barrier. The tunnel distance z used for the fit should be regarded as an effective value rather than a true measure of distance. Furthermore, it is noted that the average of 10 traces (Figure 9d) displays more noise that the average of 150 traces (Figure 9c), but the overall response is clearly reproduced in both data sets.

The situation is drastically different for the average spectra taken on the Au particles. The difference between the data and the fit as displayed in Figure 9e exhibits two systematic features, a negative curvature around 0 bias and an asymmetry with respect to the Bias = 0 axis. From the negative curvature a reduced conductivity at a low bias compared to the "normal" case is obvious. When averaging over 10 data sets no systematic steps can be seen as could be anticipated from the strong variations in position of the steps in the individual curves. Though, the steps in the individual curves lead to an increased random noise at higher absolute bias compared to the reference.

There are several possibilities that must be considered as a reason for these features. Single-electron tunnelling effects may play a role, which must be treated in the framework of a slowly reacting polarizable species around the tunnel junction. Furthermore, significant geometrical rearrangements during the scan may occur. Some influence of the chemistry seen at the tip, which consists of amino-terminated molecules on the plane surface. Carboxy groups on the particle may play a role as well. Though, one may argue that if the amino groups present on the plane surface do not lead to a response that differs significantly from the Ukraintsev picture, only small effects are to be expected from a carboxy-terminated surface.

Summary and Outlook

Gold nanoparticles functionalised with mercaptosuccinic acid were immobilized on a gold surface coated with a self-assembled monolayer consisting of 6-amino-1-hexanethiol. The formation of a well-defined geometry was followed by surface plasmon and infrared spectroscopy and proven by STM imaging.

Fluctuations in the $I(V)$ and dI/dV curves obtained with the STM under ambient conditions prevented a reliable observation of a Coulomb staircase in the system studied here. Jumps in the $I(V)$ characteristics are observed which could be interpreted in terms of a Coulomb staircase, but variations in background charge, capacitance or geometry of the double-tunnel junction can equally well account for these observations. These instabilities prevent the reproducible observation of signatures on single-electron tunnelling. A key outcome of this investigation is that we could show that the averaged response of a double-tunnel junction, although not displaying steps, significantly deviates from the response of the metal surface without particles. This was shown by fitting the data to the model proposed by Ukraintsev.[24] While the Ukraintsev model accurately describes the response of the SAM-coated surface on particles a reduced current around zero bias as well as a pronounced asymmetry of the $I(V)$ curves is observed. Although a full understanding of these effects requires further experimental and theoretical efforts, they provide a clear, robust signature for tunnelling through a surface-bound particle that is applicable to ambient conditions. These deviations probably carry a signature of molecular changes in the vicinity of the

tunnel gap and may therefore be used as nanoscopic reporters for molecular events.

Experimental Section

Substrate Preparation: Microscopy cover slides are cleaned in an Ar/O_2 Plasma (Plasma System, 200G, Technics Plasma, 1 mbar, 90% Ar/10% O_2, 5 min, 300 W) and gold is thermally evaporated on the heated (320°) substrate. A gold film of 50 nm thickness is produced at an evaporation rate of 0.1 nm s^{-1}. This leads to atomically flat Au terraces with typical dimensions of 100 nm which are sufficient for scanning tunnelling experiments.[26] The samples were immersed in a 1 mM solution in ethanol of 6-amino-1-hexanethiol (obtained in the form of its hydrochloride from Dojindo, Japan) for 4 h and subsequently rinsed with ethanol (thrice), Milli-Q water (thrice), 0.1 M HCl (once), Milli-Q water (thrice), and ethanol (once), and dried with a N_2 gun.

Deposition of Au Nanoparticles: Carboxyl-functionalised gold nanoparticles were synthesized as described by Chen et al.,[27] based on the reduction of hydrogen tetrachloroaurate(III) ($HAuCl_4 \cdot 3H_2O$ from Sigma–Aldrich, USA) by sodium borohydride in methanol using 2-mercaptosuccinic acid (MSA, obtained form Acros Organics, Belgium) as the stabilizing thiol ligand. The particle size can be easily controlled by the initial molar ratio of MSA/$HAuCl_4$. In our case, the molar ratio is 1:1. In a 500 mL 3-neck round-bottomed flask, $HAuCl_4 \cdot 3H_2O$ (1.25 mmol) in milli-Q water (5 mL) and MSA (1.25 mmol) in methanol (245 mL) were mixed and vigorously stirred for 30 min at room temperature. A freshly prepared $NaBH_4$ (12.5 mmol) in a water solution (25 mL) was added dropwise at a rate of 60–80 drops per minute, and finished in ca. 5 min. After further stirring for 1 h, the precipitate was collected and washed by a repeated centrifugation-ultrasonic dispersion process in mixed methanol/H_2O, and finally dried in vacuo. The main product was collected as 220 mg powder.

The resulting nanoparticles have diameters of 2 nm with a relatively broad size distribution as confirmed by transmission electron microscopy.

The thiol-modified substrates are immersed in a suspension containing the MSA-capped Au particles ($\approx$ 0.25 mg ml^{-1}, in pH 7.5, 0.1 M Na HEPES Buffer) for between 5 and 60 min depending on the desired particle density on the surface. After deposition, the substrate is subsequently rinsed with Na HEPES Buffer (0.1 M), NaOH solutions (0.1 M), and Milli-Q water and dried with the N_2 gun.

Scanning Tunnelling Microscopy and Spectroscopy: Scanning tunnelling microscopy was performed with a homebuilt scanhead in combination with a commercial controller (RHK SPM 1000). For imaging, the "constant current" mode was used. $I(V)$ spectra that can be unambiguously assigned to topographic features in the image were obtained by interrupting image acquisition and taking the $I(V)$ curves along some preset lines, yielding a complete image with a rectangular grid where $I(V)$ curves were taken. dI/dV spectra were obtained simultaneously by superimposing a sinusoidal modulation on the bias voltage (amplitude 15 mV, frequency 10–40 kHz), which was fed into a lock-in amplifier (Femto, LIA-MVD-200).

Monolayer Analysis: Surface plasmon spectroscopy in the Kretschmann-configuration was performed on a homebuilt set-up, using a HeNe Laser (λ = 633 nm) as light source. This technique, which is described in detail in ref.[28] allows for the monitoring of the thickness of a homogeneous adlayer of known dielectric response from angle-dependent reflectivity measurements. For the deposition of MSA-capped Au particles the coverage as a function of time can be monitored up to an unknown scaling factor, which must be determined by complementary methods. The angle of the reflectivity minimum was monitored as a function of time by measuring three values for each point of the Reflectivity for θ at the last determined minimum position, slightly above and slightly below. The new minimum position was determined as the minimum of a parabola through these three points.

Infrared spectroscopy was performed with a Magna 850 Series II FTIR spectrometer (Nicolet) under grazing incidence.

Acknowledgments

We are grateful to H. Schniepp for supporting us with his scanning probe image viewer and including our file format to it. We acknowledge financial support from the DFG- Schwerpunktprogramm "Hableiter- und Metallcluster als Bausteine für organisierte Strukturen" (DFG-SPP 1072).

[1] A. N. Korotkov, *Coulomb Blockade and Digital Single-Electron Devices*, IUPAC, **1997**.
[2] A. E. Hanna, M. Tinkham, *Phys. Rev. B* **1991**, *44*, 5919.
[3] J. W. Gerritsen, S. E. Shafranjuk, E. J. G. Boon, G. Schmid, H. van Kempen, *Europhys. Lett.* **1996**, *33*, 279.
[4] R. S. Ingram, M. J. Hostetler, R. W. Murray, T. G. Schaaff, J. T. Khoury, R. L. Whetten, T. P. Bigioni, D. K. Guthrie, P. N. First, *J. Am. Chem. Soc.* **1997**, *119*, 9279.
[5] M. Y. Han, L. Zhou, C. H. Quek, S. F. Y. Li, W. Huang, *Chem. Phys. Lett.* **1998**, *287*, 47.
[6] M. Dorogi, J. Gomez, R. Osifchin, R. P. Andres, R. Reifenberger, *Phys. Rev. B* **1995**, *52*, 9071.
[7] R. P. Andres, T. Bein, M. Dorogi, S. Feng, J. I. Henderson, C. P. Kubiak, W. Mahoney, R. G. Osifchin, R. Reifenberger, *Science* **1996**, *272*, 1323.
[8] B. Wang, H. Q. Wang, H. X. Li, C. G. Zeng, J. G. Hou, X. D. Xiao, *Phys. Rev. B* **2001**, 63.
[9] L. E. Harrell, T. P. Bigioni, W. G. Cullen, R. L. Whetten, P. N. First, *J. Vac. Sci. Technol. B* **1999**, *17*, 2411.
[10] L. C. Brousseau, Q. Zhao, D. A. Shultz, D. L. Feldheim, *J. Am. Chem. Soc.* **1998**, *120*, 7645.
[11] W. P. McConnell, L. C. Brousseau, D. L. Feldheim, *Abstracts Of Papers Of The American Chemical Society* **2000**, *219*, U114.
[12] H. Osman, J. Schmidt, K. Svensson, R. E. Palmer, Y. Shigeta, J. P. Wilcoxon, *Chem. Phys. Lett.* **2000**, *330*, 1.
[13] L. F. Chi, M. Hartig, T. Drechsler, T. Schwaack, C. Seidel, H. Fuchs, G. Schmid, *Applied Physics A-Materials Science & Processing* **1998**, *66*, S187.
[14] G. Schmid, G. L. Hornyak, *Current Opinion in Solid State & Materials Science* **1997**, *2*, 204.
[15] W. P. McConnell, J. P. Novak, L. C. Brousseau, R. R. Fuierer, R. C. Tenent, D. L. Feldheim, *J. Phys. Chem. B* **2000**, *104*, 8925.
[16] C. Schoenenberger, H. van Houten, C. W. J. Beenakker, *Physica B* **1993**, *189*, 218.
[17] R. M. Silverstein, C. G. Bassler, T. C. Morill, *Spectrometric Identification of Organic Compounds*, 5 ed., John Wiley and Sons, **1995**.
[18] A. N. Parikh, D. L. Allara, I. B. Azouz, F. Rondelez, *J. Phys. Chem.* **1994**, *98*, 7577.
[19] J. Tien, A. Terfort, G. M. Whitesides, *Langmuir* **1997**, *13*, 5349.
[20] J. M. Brockman, A. G. Frutos, R. M. Corn, *J. Am. Chem. Soc.* **1999**, *121*, 8044.
[21] M. Sprik, E. Delamarche, B. Michel, U. Rothlisberger, M. L. Klein, H. Wolf, H. Ringsdorf, *Langmuir* **1994**, *10*, 4116.
[22] M. L. Wallwork, D. A. Smith, J. Zhang, J. Kirkham, C. Robinson, *Langmuir* **2001**, *17*, 1126.

[23] H. A. Wierenga, L. Soethout, J. W. Gerritsen, B. E. C. van de Leemput, H. van Kempen, G. Schmid, *Adv. Mater.* **1990**, *2*, 482.
[24] V. A. Ukraintsev, *Phys. Rev. B* **1996**, *53*, 11176.
[25] H. Stöcker, *Taschenbuch der Physik*, 3 ed., Harri Deutsch, Frankfurt a. M., **1998**.
[26] J. Hwang, M. A. Dubson, *J. Appl. Phys.* **1992**, *72*, 1852.
[27] S. H. Chen, K. Kimura, *Langmuir* **1999**, *15*, 1075.
[28] W. Knoll, *Ann. Rev. Phys. Chem.* **1998**, *49*, 569.
Received: March 29, 2005
Published Online: August 1, 2005

